Progress In Electromagnetics Research, Vol. 137, 275–292, 2013

A MINIATURIZED TRIPLE-BAND METAMATERIAL ANTENNA WITH RADIATION PATTERN SELECTIVITY AND POLARIZATION DIVERSITY

H.-X. Xu[1, *], G.-M. Wang[1], and M.-Q. Qi[2]

[1]Missile institute, Air Force Engineering University, Xi'an 710051, China

[2]State Key Laboratory of Millimeter Waves, Southeast University, Nanjing 210096, China

Abstract—A novel triple-band single-fed compact microstrip antenna with varied polarization states and radiation patterns is proposed based on two-dimensional artificial metamaterial transmission line (TL). The TL element is composed of complementary split ring resonators (CSRRs) etched in the ground plane and a capacitive gap embedded in the stepped-impedance conductor line. By inserting a 2×2 array of the original element in conventional patch and feeding the resultant structure with an annular-ring slot along the diagonal, an antenna working in three resonant modes ($n = -1$, $n = 0$, and $n = +2$) is engineered at three specific well-separated frequencies $f_{-1} = 1.5$, $f_0 = 2.4$ and $f_{+2} = 3.5\,\text{GHz}$, respectively. As a result, both the numerical and experimental results illustrate that the antenna exhibits a patch-like radiation with pure linear polarization in the $n = -1$ mode, a monopolar radiation with circular polarization in the $n = 0$ and also an asymmetric quasi monopolar radiation with a hybrid linear polarization in the $n = +2$ mode. The antenna features compact whose patch occupying only an area of $0.246\lambda_0 \times 0.246\lambda_0 \times 0.03\lambda_0$ at f_{-1} and exhibits groups of advantages such as high radiation efficiency. Moreover, the proposed prescription, free of any metallic via, perturbation structure and complicated feeding network, is of practical value and opens an alternative avenue toward new types of antenna with agile polarization capability and versatile radiation patterns.

Received 10 August 2012, Accepted 24 September 2012, Scheduled 21 February 2013

* Corresponding author: He-Xiu Xu (hxxuellen@gmail.com).

1. INTRODUCTION

Recent burgeoning developments toward electromagnetic (EM) metamaterials have intrigued a great impetus and a renewed interest in the antenna discipline [1–7]. Microstrip antenna is of particular interest and preferable due to their features of low profile, light weight, easy fabrication, low cost and compatibility with the integrated circuit technology in practice. This is especially true for the circularly polarized (CP) microstrip antenna which owns additional advantages of imposing less strict restrictions on orientation of the transmitter and receiver and mitigative multi path effects. A survey of recent literature indicates that a considerable amount of efforts have been devoted to the antennas with CP, for instance, CP antennas for bandwidth enhancement by using left handed (LH) metamaterial transmission line (TL) [8] and reactive impedance substrates [9], respectively, CP antennas with gain and directivity enhancement [10–13], omnidirectional radiations [14–16] and even dual-band or multi-frequency operation with radiation pattern selectivity and polarization diversity [16–25].

Among them, the multiband antennas [16–25] with one or more CP bands have generated much attention because the multifunctional systems exhibit the benefits of high stability, reliability and integrity. Although these antennas present a miniaturized layout at the lowest resonant mode and decent CP radiation performances with good axial ratios (ARs), some of them are confined to mushroom structure which provides the shorted LH stub inductor through drilling via holes [16–19]. In this case, large currents concentrate around the vias which are lossy conductors, generating considerable losses in the structure. Accordingly, the antenna's gain and radiation efficiency may be degraded by a few percentages. Recently, a metamaterial branch-line coupler [20] and a power divider [21] were utilized for dual-band CP antennas with dual-fed technology. Although the excitation of the two orthogonal modes with 90° phase difference for CP is convenient and straightforward, the complicated feeding network occupies a large area which conflicts with currently increasing demand on compactness. One-dimensional (1D) complementary split ring resonators (CSRRs) [22, 23] and complementary spiral resonators (CSRs) [24] in terms of single negative metamaterial resonator have been explored for CP antennas due to the anistropic property of CSRRs and CSRs, however, the two-dimensional (2D) CSRRs in terms of double-negative resonant-type artificial TL have never been reported for a CP antenna.

The goal of this paper is thus to provide a alternative and

improved strategy not only to address the loss and gain issue but also to obtain good antenna performances such as radiation pattern selectivity and polarization diversity [26] over multibands. A miniaturized single-fed triple-band antenna operating in $n = -1$, $n = 0$, and $n = +2$ mode and exhibiting both CP and LP characteristics is proposed based on the 2D CSRRs-loaded metamaterial TL which is also known as composite right left handed (CRLH) TL. To provide a better understanding about the functions of the CSRRs-loaded metamaterial, the TL approach is introduced for the design and characterization.

2. THEORY, FUNDAMENTALS AND ANTENNA DESIGN

2.1. Metamaterial Structure, Equivalent Circuit Model and Theory

Figure 1 depicts the geometry and corresponding equivalent circuit model of the proposed 2D CSRRs-loaded metamaterial transmission line. As is shown, the 2D TL element comprises four 1D CSRRs-loaded TL elements in the two orthogonal principal directions with each element intersecting at the middle point, respectively. By arranging periodically the 2D element, the resulting infinite planar metamaterial TL can be engineered. The EM characteristic of the high-low stepped-impedance conductor line is employed from the point of view of easy

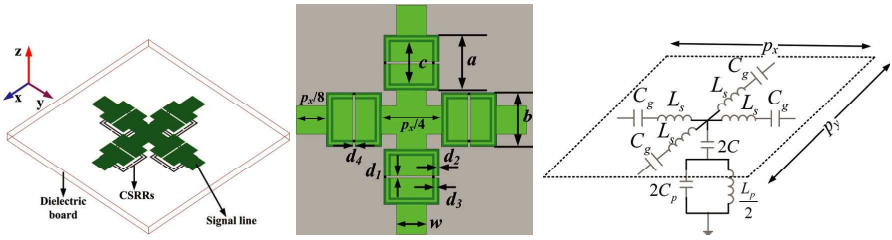

(a) (b) (c)

Figure 1. Geometry and corresponding equivalent circuit model of the 2D CSRRs-loaded metamaterial TL, (a) perspective view; (b) top-and-bottom view as well as the illustration of geometrical dimensions; (c) circuit model. The capacitive gaps are etched on the low-impedance conductor strip (depicted in blue) beneath which, the CSRRs (depicted in dark) are etched on the ground plane (depicted in grey). The elaborate geometrical parameters are: $d_1 = d_2 = d_3 = d_4 = 0.2\,\text{mm}$, $a = b = 4.8\,\text{mm}$, $w = 2.6\,\text{mm}$, and $c = 3.6\,\text{mm}$.

and broadband impedance match. The high-impedance signal lines in both ends utilized to connect adjacent cells are $p_x/8$, where p_x is the total dimension (periodicity) of the cell in x-direction and is identical with that in y-direction. Therefore, the proposed metamaterial TL is isotropic due to the four-fold rotational symmetry, and the lumped elements in the equivalent circuit model are two times that of the 1D case. In like manner, the impinging of CSRRs etched in the ground to the axial (z-directed) time-varying electric-field components is responsible for the parallel resonant tank formed by L_p and C_p in the shunt branch, and in turn the negative electric response, whereas the capacitive gap C_g and the inherent parasitic right handed (RH) inductance L_s are accounting for the negative magnetic permeability. Remark that capacitor C comprises not only the RH parasitic line capacitance but also the electric coupling between signal lines and CSRRs.

To gain a better understanding of the principle, we immediately deduce the analytic dispersion diagram along the full Brillouin zone by adopting the Bloch-Floquet periodic boundary condition to the isotropic unit-cell circuit.

$$k_x = \frac{j}{p}\log\left\{\frac{(2+L)-\sqrt{(2+L)^2-4}}{2}\right\}, \tag{1}$$

$$\Gamma\text{-}X : 0 < k_x p < \pi; \quad k_y p = 0$$

$$k_y = \pi + \frac{j}{p}\log\left\{\frac{(6+L)-\sqrt{(6+L)^2-4}}{2}\right\}, \tag{2}$$

$$X\text{-}M : k_x p = \pi; \quad 0 < k_y p < \pi$$

$$k_i = 3\pi - \frac{j}{p}\log\left\{\frac{(4+L)-\sqrt{(4+L)^2-16}}{4}\right\} \tag{3}$$

$$M\text{-}\Gamma : 0 < k_x p = k_y p < \pi; \quad i = x \text{ and } y$$

Note that k_x and k_y are complex wave numbers in the x- and y-direction, respectively and Γ, X, M are the symmetry points ($k_x p = k_y p = 0$), ($k_x p = \pi$, $k_y p = 0$) and ($k_x p = k_y p = \pi$), respectively. Here, L is formulated as

$$L = \frac{4C}{C_g}\left[1-\left(\frac{\omega}{\omega_{se}}\right)^2\right]\left[1-\left(\frac{\omega}{\omega_p}\right)^2\right]\Big/\left[1-\left(\frac{\omega}{\omega_{sh}}\right)^2\right] \tag{4}$$

where ω_{se}, ω_{sh} and ω_p are the resonant frequencies of the series branch, shunt branch and parallel resonant tank, respectively.

$$\omega_{se} = \omega_{\Gamma 2} = 2\pi f_{se} = 1/\sqrt{L_s C_g}, \tag{5a}$$

$$\omega_{sh} = 2\pi f_{sh} = 1/\sqrt{L_p(C + C_p)}, \tag{5b}$$

$$\omega_p = \omega_{\Gamma 1} = 2\pi f_p = 1/\sqrt{L_p C_p}. \tag{5c}$$

The balanced condition occurs when $\omega_{se} = \omega_p$, where a seamless transition is appreciated between the LH and RH band. Otherwise an inhibition interval is perturbed in the passband. For theoretical characterization, the lumped elements shown in the caption of Fig. 2 are retrieved. Then these circuit elements are implanted into Eqs. (1)–(3) by combining Eqs. (4) and (5) to theoretically calculate the dispersion diagram. The commonly available 1 mm-thick F4B substrate with dielectric constant $\varepsilon_r = 2.65$, and loss tangent $\tan\delta = 0.001$ is adopted for the characterization. Fig. 2 illustrates the theoretical and full-wave dispersion diagram through eigenmode analysis performed in the commercial finite-element-method EM solver Ansoft HFSS. In the eigenmode analysis, one unit cell is enclosed in a 10 mm-height air box with the top and bottom boundary along z-axis assigned as perfectly matched layers and the four boundaries along x- and y-direction assigned as master/slave boundary (periodical boundary). Follow the figure, an excellent agreement is clearly observed between both results. The slight deviation is attributable to the mutual coupling and edge effects introduced by the densely arranged four-fold symmetrical CSRRs and also to the computing tolerances induced by the meshing variations. Nevertheless, the coupling effects are impossible to be sufficiently incorporated in a simple circuit. As is expected, the backward-wave propagation

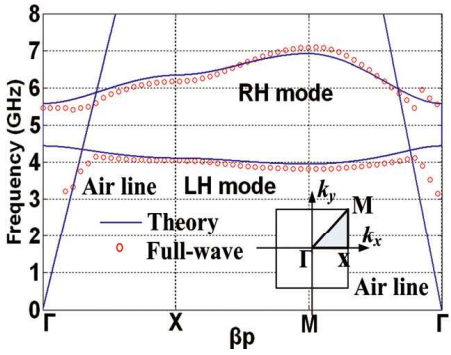

Figure 2. Dispersion diagram of the proposed 2D metamterial TL element obtained from eigenmode analysis and TL theory. The lumped elements are retrieved as $L_s = 2.57$ nH, $C_g = 0.32$ pF, $C = 2.9$ pF, $C_p = 3.34$ pF and $L_p = 0.39$ nH at 6 GHz.

(LH characteristic) with antiparallel phase (ω/β) and group ($\partial\omega/\partial\beta$) velocities is clearly shown in the frequency region from 3.94 to 4.46 GHz (zeroth-order resonance ω_p) and a stopband interval is perturbed from 4.46 to 5.5 GHz.

2.2. Antenna Layout, Fundamentals and Design

Now that it has been well established that the proposed 2D metamaterial TL exhibits fundamental LH characteristics in the LH resonant mode, it is especially interesting to explore the radiation characteristics of the antenna made of these electrically small elements which are able to provide a degree of miniaturization on antenna size. Since it was demonstrated in previous work that additional antenna aperture in the transverse direction benefited considerably the antenna gain and radiation efficiency [27], the 2D topology is still utilized for the CP antenna in this particular design. However, the operating mechanism is completely different which will be elucidated later. Fig. 3 depicts the corresponding antenna layout. As can be seen, the antenna is constructed by inserting a 2×2 array of the proposed 2D TL element into the conventional RH patch to inspire the microstrip antenna, enabling the newly fashioned open-ended RH + CRLH + RH structure a hybrid resonator. For the sake of CP radiation at some specific frequency, the antenna is fed by a single coaxial probe (diameter of

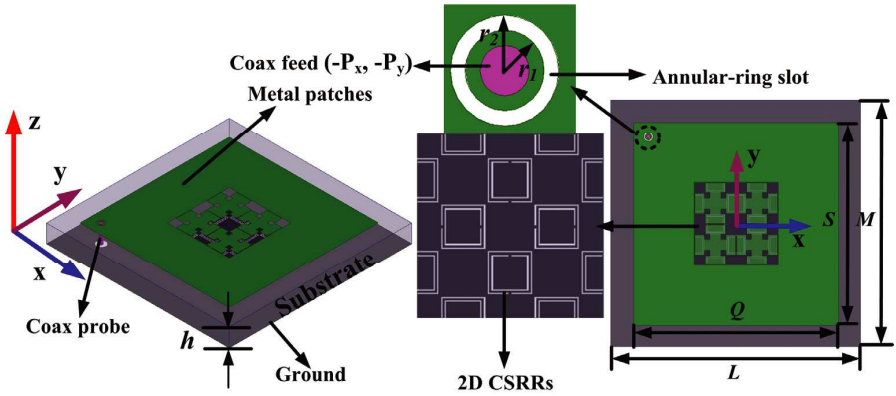

Figure 3. Perspective view as well as top-and-bottom view of the proposed compact triple-band antenna based on the 2D resonant-type metamaterial TL shown in Fig. 1. The geometrical parameters are designed as: $L = M = 60\,\text{mm}$, $P_x = P_y = 21\,\text{mm}$, $Q = S = 49\,\text{mm}$, $w = 2.6\,\text{mm}$, $h = 6\,\text{mm}$, $r_1 = 0.9\,\text{mm}$, and $r_2 = 1.2\,\text{mm}$.

$d = 1.2\,\text{mm}$) located at the position $(-P_x, -P_y)$ on the 45° diagonal to excite the two near-degenerated orthogonal modes with 90° phase difference. No perturbation structure such as truncated patch is necessary [18]. The antenna layout is built on the inexpensive F4B substrate with $\varepsilon_r = 2.65$, $h = 6\,\text{mm}$ and loss tangent $\tan\delta = 0.001$. Owing to the thick substrate, a capacitive concentric-ring slot (annular-ring slot) [28] is employed to counteract the large imaginary part of impedance (namely the inductive effect of the probe feeding) for an easy impedance match.

Since the antenna is fed along the 45° diagonal, the propagation constant β_n^{LH} calculated using Eq. (3) in the Γ-M section of the Brillouin zone contains both x and y-directed components. This feature distinguishes the design of the CP antenna from that of LP antenna on the basis of the TL theory. This is because the antenna aperture in x and y directions both contributes the LH performance in this work, whereas only the longitudinal antenna aperture plays a dominant role in affecting the LH characteristic of LP antenna which is excited by a probe along either x or y axis. To provide fundamentals associated with multifrequency antenna and individual control over the multi-resonant modes in practical design, analytical expressions are derived and quantitative analyses are also performed. For convenience, the length of each RH section and each 1D LH cell in CRLH section composed of N cells along the diagonal are defined as $d/2$ and ρ, respectively. The overall eigenfrequencies in the hybrid resonator satisfy the resonant condition.

$$\beta_n L = \beta_n^{RH} d/2 + \beta_n^{LH} \rho N + \beta_n^{RH} d/2 = n\pi \tag{6}$$

Note that β_n^{RH} is the phase constant of RH patch along the diagonal and formulated as a function of L_R and C_R associated with the per-unit-length inductance and capacitance, respectively.

$$\beta_n^{RH} = \omega\sqrt{L_R C_R} \tag{7}$$

L is the equivalent dimension of the total hybrid resonator along the diagonal, whereas n is the resonant mode (indices) and fulfills the constraint$n = -N+1, -N+2, \ldots 0, 1, 2, \ldots N-2, N-1$. The impedance Z_{RH} and electrical length ($\beta_n^{RH} d = \beta d$) of the RH patch can be assessed from the physical layout according to the classical analytic formulas. Fig. 4 depicts the theoretical dispersion diagram of the hybrid resonator under different electrical length of the RH patch by combining Eqs. (3), (6) and (7). Notice that βd is evaluated at 1.39 GHz and Z_{RH} is preserved as $45\,\Omega$ in all cases. The circuit elements of the metamaterial TL element shown in the caption of the figure are arbitrarily selected without loss of generality. Following the figure where the resonant index is also identified, it can be easily

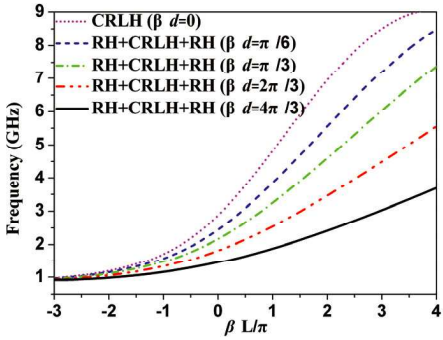

Figure 4. Theoretical dispersion relation of the hybrid resonator under different cases. The circuit parameters of the metamaterial TL element are selected as $L_s = 1.75\,\text{nH}$, $C_g = 1.75\,\text{pF}$, $C = 1\,\text{pF}$, $C_p = 1.75\,\text{pF}$ and $L_p = 1.75\,\text{nH}$.

learned that the slope of the dispersion curve of the hybrid resonator reduces continuously as βd increases from $\pi/6$ to $4\pi/3$. This results in lower resonant frequencies and small frequency interval between the resonant modes and thus enables to provide a degree of miniaturization on antenna layout. Therefore, the proportion of the RH patch to the LH metamaterial TL can be monitored to arbitrarily control the operating frequencies of a multiband antenna, which renders an additional degree of freedom. This conclusion coincides well with that has been drawn in [27] for LP antenna whose dominant propagation component is either along x- or y-direction. However, it is worth to declare that Z_{RH} poses very weak influence on the resonance frequency.

3. ILLUSTRATIVE RESULTS AND DISCUSSIONS

Following the fundamentals, the RH patch is cautiously optimized to locate the three specific operating frequencies at three resonant modes in the dispersion diagram, respectively, i.e., the band near the global positioning system (GPS, 1575 MHz) f_{-1} in $n = -1$ mode, the Bluetooth band (2.4 GHz) f_0 in $n = 0$ mode and the Wimax band (3.5 GHz) f_{+2} in $n = +2$ mode. The geometrical parameters of the designed multifrequency antenna are shown in the caption of Fig. 3. For verification, the present antenna is fabricated and assembled with the prototype can be appreciated in Fig. 5, and is measured with return loss recorded through a N5230C vector network analyzer while radiation patterns through the far-field measurement system in

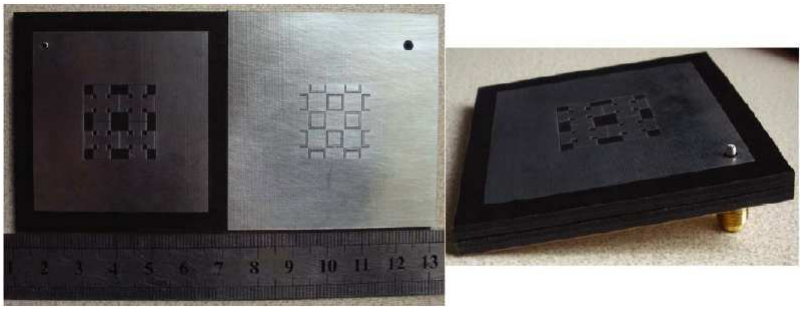

(a) (b)

Figure 5. Photograph of the fabricated prototype. (a) Top and bottom view as well as (b) perspective view of the assembled antenna based on the metamaterial hybrid resonator.

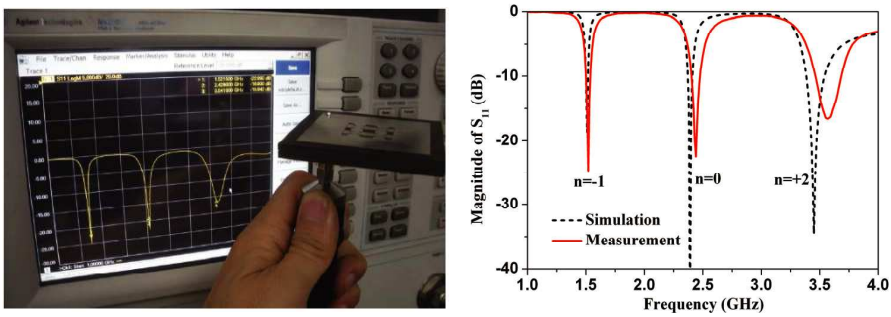

(a) (b)

Figure 6. Simulated and measured return loss of the proposed antenna based on the metamaterial hybrid resonator. (a) Illustration of the measurement; (b) comparison between simulation and measurement.

an anechoic chamber. Since the substrate of expected thickness is not available in manufacture, two layers of 3 mm-thick substrate with identical dielectric constant are bonded together to replace the thick one in the experiment. A hot press is performed to drive the air between the two substrates.

Figure 6 displays the simulated (characterized in HFSS) and measured return loss against frequency. As is appreciated, an excellent agreement of results between simulation and measurement is unambiguously observed except for a slight frequency shift upward

in the higher band in the measurement case. Moreover, both numerical and experimental results illustrate clearly three resonant modes which can be identified from the reflection dips. The measured return losses are evaluated orderly as −24.6 dB, −22.4 dB and −16.58 dB at $f_{-1} = 1.52$, $f_0 = 2.44$ and $f_{+2} = 3.57$ GHz, respectively, indicating perfect impedance matching performances and an efficient design. Note that the $n = +1$ mode is not excited and the above resonant modes will be justified and validated through both the electric field distribution analysis and the far-filed radiation characteristics in the upcoming section. The absolute 10 dB impedance bandwidth is measured as 40, 80 and 230 MHz, corresponding to 2.63%, 3.28%, and 6.44% fractional bandwidth, respectively. In addition to the aforementioned frequency shift, the measured bandwidth is a little broader than that in the simulation. These deviations can be associated with the tolerances that are inherent in the fabrication process. This is especially true in this particular design due to the introduced air layer between two substrate boards and the slight misalignment of the CSRRs and gaps in the experiment. The air layer reduces the dielectric constant, and thus degrades the quality factor and pushes up the operating frequency accordingly.

To further validate these resonant modes, Figs. 7 and 8 depict the HFSS-simulated electric field distribution and the three-dimensional far-field radiation patterns of the proposed antenna at three operating frequencies. It is worth pointing out the electric fields should be observed along the 45° diagonal of the entire RH patch and CRLH section since the antenna is diagonally excited. Following Fig. 7, very obvious uniform (in-phase) electric fields are obtained along the 45° diagonal at $f = 2.4$ GHz, implying that an infinite wavelength is supported at this zeroth-order resonant (ZOR) mode, whereas the

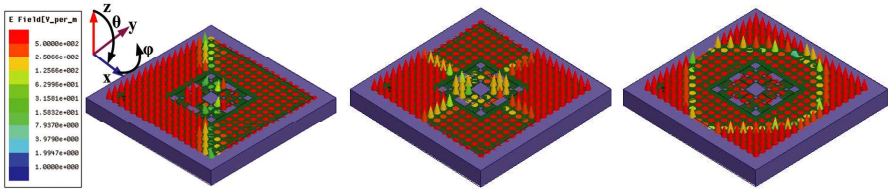

(a) (b) (c)

Figure 7. Electric field distribution on the top layer of the proposed antenna based on the metamaterial hybrid resonator (a) in $n = -1$ mode ($f_{-1} = 1.51$ GHz); (b) $n = 0$ mode ($f_0 = 2.4$ GHz) and (c) $n = +2$ mode ($f = 3.52$ GHz).

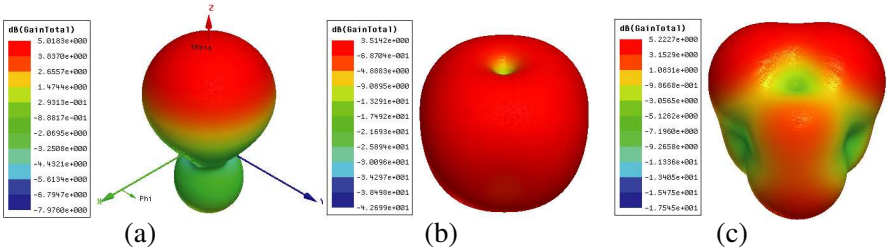

(a) (b) (c)

Figure 8. Far-field radiation patterns of the proposed antenna based on the metamaterial hybrid resonator (a) in $n = -1$ mode; (b) $n = 0$ mode and (c) $n = +2$ mode.

electric fields at both sides of the 45° diagonal are 180° out-of-phase at the fundamental frequency $f_{-1} = 1.51$ GHz corresponding to a half-wavelength distribution. As a consequence, a patch-like radiation pattern and a monopolar radiation pattern (null radiation at the broadside direction) are expected at 1.51 and 2.4 GHz, respectively in Fig. 8. It should be noted that the field intensity in the metamaterial region outside the microstrip patch are very weak and the phase of fields still takes the half-wavelength distribution at 2.4 GHz along two principal axes, whereas in contrast it is uniform at the negative order resonant mode 1.51 GHz.

As to the last operating frequency around 3.5 GHz, the direction of the fields plotted in Fig. 7(c) shifts twice along the diagonal and still distributes uniformly at both ends of the diagonal (one-wavelength resonance), enabling a higher positive second order resonant mode $n = +2$. On the other hand, the uniform field distribution along four patch edges implies that the $n = +2$ mode has been split into two modes with equal magnitude in two orthogonal polarization, resembling two identical antennas placed in orthogonal orientation. Since these divisive orthogonal modes do not radiate at broadside, see Fig. 8(c) due to the nonuniform aperture phase distribution, they are unable to provide a CP radiation pattern. Instead, the peak radiation pattern encounters an inclined angle around $\theta = -38°$ in *xoz* and *yoz* plane, respectively and thus gives rises to the unsymmetrical quasi monopolar radiation pattern which can be further confirmed from the measured results shown in Fig. 10. Therefore, the antenna performs specific functions in the $n = +2$ mode to enable the radiating structure to be a hybrid LP antenna, which will be further illustrated later in detail.

Figure 9 depicts the HFSS simulated ARs and 2D radiation patterns versus the elevation angle θ (Theta) at some selected specific

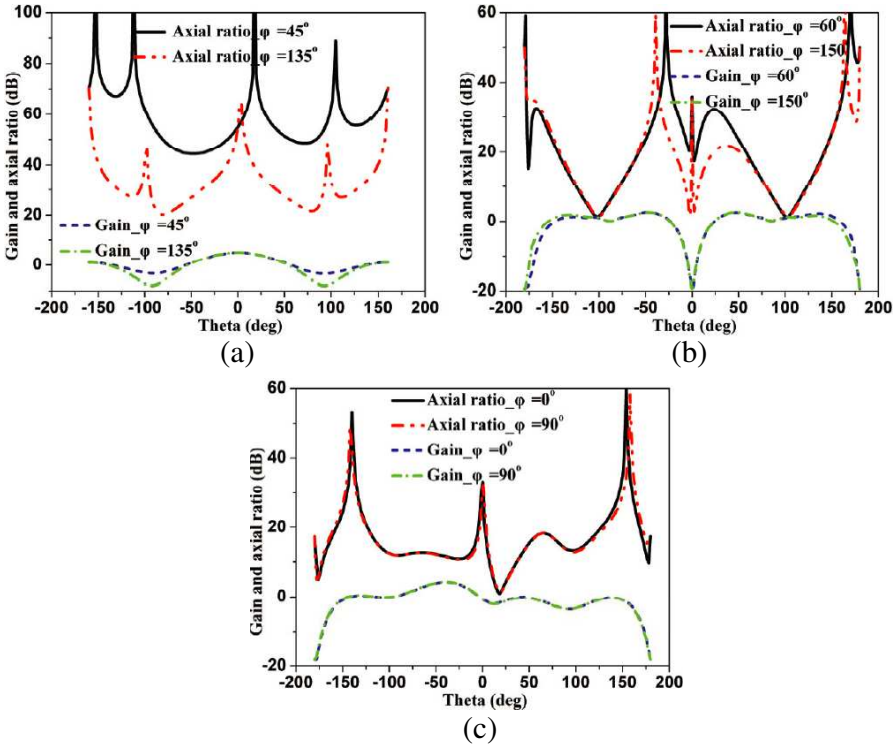

Figure 9. ARs and radiation patterns of the proposed antenna based on the metamaterial hybrid resonator for (a) $n = -1$ mode; (b) $n = 0$ mode; and $n = +2$ mode.

plane. Referring to the figure, one can easily find that the antenna emits a pure LP radiation pattern with AR on the order of 55 dB at $f_{-1} = 1.51$ GHz, while a CP radiation with AR near 1.28 dB at $f_0 = 2.4$ GHz and a hybrid LP radiation at $f_{+2} = 3.52$ GHz. The AR (evaluated at the peak radiation point) is obtained around 11.5 dB at 3.52 GHz, suggesting a LP radiation with imperfect polarization purity due to the two divisive orthogonal LP modes. Remark that the antenna is polarized along the $\varphi = 45°$ diagonal in $n = -1$ mode, whereas two near-degenerated orthogonal modes with 90° phase difference are along the $\varphi = 60°$ and $\varphi = 150°$ plane, respectively in $n = 0$ mode. In contrast, the peak radiation still occurs in the two principal plane of $\varphi = 0°$ and $\varphi = 90°$ in $n = +2$ mode. The altered LP orientation in $n = -1$ mode and CP orientation in $n = 0$ mode are attributable to the capacitive gaps in two orthogonal directions. The currents excited

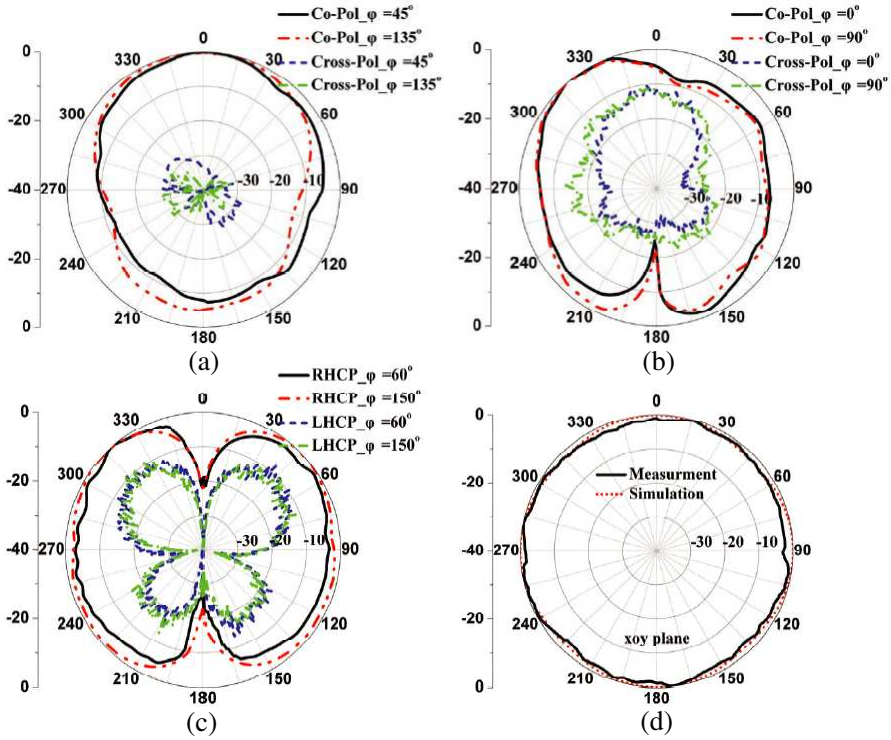

Figure 10. Measured radiation patterns of the proposed antenna based on the metamaterial hybrid resonator for (a) $n = -1$ mode; (b) $n = +2$ mode; as well as (c), (d) $n = 0$ mode.

by the CSRRs flow along these gaps and make the structure function as a monopole placed along the gap [29]. As a consequence, at least two monopoles are orthogonally distributed. These aspects distinguish the characteristics of present antenna from those of previous antennas inspired from mushroom-loaded LH TLs [18, 19].

For verification, the far-field radiation patterns are measured and plotted in two principal planes in Fig. 10. As can be evidently observed, the experimental results are in excellent consistency with the numerical ones shown in Fig. 8. A patch-like, a monopolar, and an unsymmetrical quasi monopolar radiation pattern are clearly obtained in $n = -1$, $n = 0$ and $n = +2$ mode, respectively. The etched CSRRs slots in the ground give rise to the bi-directional radiation in all resonant modes. The low cross polarization level which is more than 30 dB lower than the co-polarization in the $n = -1$ mode should

be highlighted, further confirming the pure LP radiation. In addition, the LH CP (LHCP, cross polarization) is also achieved almost 30 dB lower than the RH CP (RHCP, co-polarization) in $n = 0$ mode, indicating a fairly good CP purity, whereas a cross-polarization purity of near 13.5 dB is expected in the hybrid resonant mode $n = +2$. An intriguing property of the antenna should be the omindirectional radiation (the measured power intensity fluctuates within 3 dB) in *xoy* plane in $n = 0$ mode, which would afford large service area in practice. For a comprehensive study, the effects of the ground on the antenna performances are also numerically investigated. Plus the case of the infinite ground, bigger and smaller ground than that in current case, total four cases are considered. For a fair comparison, the residual conditions are completely the same. Numerical results indicate that the antenna gain and cross-polarization purity are slightly improved when the ground extends in some specific range while are almost constant when the ground further increases to infinite. In either case, the other performances such as the fundamental working modes and the shape of radiation patterns are almost fixed.

Figure 11 compares the simulated and measured ARs against frequency in the two vertical principal planes ($\varphi = 60°$ and $\varphi = 150°$) defined in the aforementioned section in $n = 0$ mode. To provide a comprehensive study, the polarization states in the horizontal *xoy* plane are also incorporated in this figure. Following Fig. 11(a), a good agreement of results between simulation and measurement is evidenced, suggesting fairly good CP characteristics with a measured 3 dB AR bandwidth (2.32–2.56 GHz) of 9.84%. From Fig. 11(b),

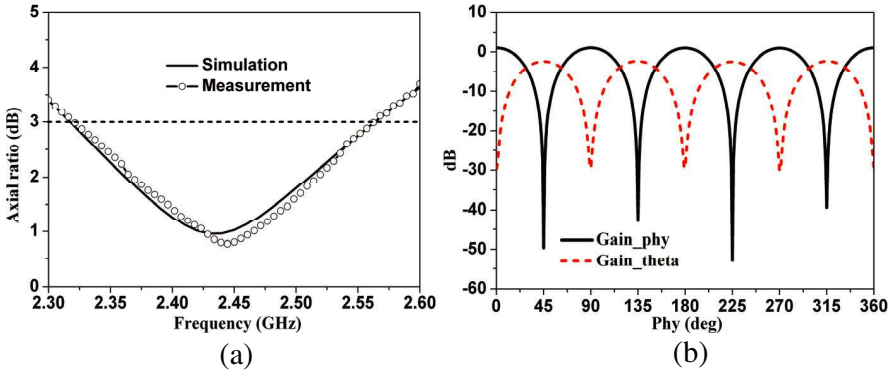

Figure 11. Comparison of (a) the ARs between the simulation and measurement, and (b) the polarization states in *xoy* plane in $n = 0$ mode.

Table 1. Comprehensive measured behaviors of the proposed antenna in different resonant modes.

Modes	Center freq.(GHz)	Polarization state	S_{11}(dB)	Gain (dB)	Rad. Effi. (%)	Antenna size (λ_0)	Principal plane	Bandwidth (S_{11}/AR, %)
n=-1	1.52	LP	–24.6	4.93	89.9	0.248×0.248	φ=45° and φ=135°	2.63/-
n=0	2.44	CP	–22.4	2.85	91.8	0.398×0.398	φ=60° and φ=150°	3.28/9.84
n=+2	3.57	Hybrid LP	–16.58	5.12	97.6	0.583×0.583	φ=0° and φ=90°	6.44/-

we learn that the polarization state with Gain_phy and Gain_theta occurring by turns changes every 45° of the azimuth angle. The reason is the same due to the 2D CSRRs and gaps discussed previously. The detailed measured behavior of the proposed antenna is summarized in Table 1. Note that the antenna size is characterized by the ratio of the area encompassed by the top patch to the wavelength in free space. To the authors' best knowledge, the proposed antenna achieves one of the best performances such as the antenna gain and radiation efficiency while is with a compact prototype occupying one of the best size reductions (75.4% smaller than conventional half-wavelength microstrip antenna evaluated at 1.52 GHz) among the available metamaterial antennas based on mushroom structure [16–19].

4. CONCLUSION

A novel triple-band antenna based on CSRRs-loaded 2D metamaterial TL has been systematically studied in this paper. Theoretical analysis based on Bloch theory and eigenmode analysis is also performed for characterization and design. Both numerical and experimental results illustrate that the antenna operating in $n = -1$, $n = 0$, and $n = +2$ resonant modes exhibits a patch-like, a monopolar and an unsymmetrical quasi monopolar radiation pattern covering the GPS, Bluetooth, and Wimax band, respectively. Further results demonstrate that the antenna provides orderly pure LP, fairly nice CP and hybrid LP radiation patterns in these three resonant modes. The abnormal EM radiation behavior has been discussed in depth from a physical insight. The good performances of the antenna predict promising applications in mobile and wireless local area network (WLANs) systems which require compact antennas with radiation pattern selectivity and polarization diversity.

ACKNOWLEDGMENT

This work is supported by the National Natural Science Foundation of China under Grant No. 60971118, and is also supported by the Innovation Foundation for Postgraduate's Dissertation of Air Force Engineering University under Grant No. DY12101. The authors should deliver their sincere gratitude to the anonymous reviewers for their constructive comments.

REFERENCES

1. Engheta, N. and R. W. Ziolkowski, *Electromagnetic Metamaterials: Physics and Engineering Explorations*, Wiley, Hoboken, NJ, 2006.
2. Eleftheriades, G. V. and K. G. Balmain, *Negative Refraction Metamaterials: Fundamental Principles and Applications*, Wiley, Hoboken, NJ, 2005.
3. Caloz, C. and T. Itoh, *Electromagnetic Metamaterials: Transmission Line Theory and Microwave Applications: The Engineering Approach*, Wiley, Hoboken, NJ, 2006.
4. Marques, R., F. Martin, and M. Sorolla, *Metamaterials with negative parameters: Theory, Design, and Microwave Applications*, Wiley, Hoboken, NJ, 2008.
5. Alici, K. B., A. E. Serebryannikov, and E. Ozbay, "Radiation properties and coupling analysis of a metamaterial based, dual polarization, dual band, multiple split ring resonator antenna," *Journal of Electromagnetic Waves and Applications*, Vol. 24, Nos. 8–9, 1183–1193, 2010.
6. Valagiannopoulos, C. A., "Electromagnetic scattering of the field of a metamaterial slab antenna by an arbitrarily positioned cluster of metallic cylinders," *Progress In Electromagnetics Research*, Vol. 114, 51–66, 2011.
7. Du, G.-H., X. Tang, and F. Xiao, "Tri-band metamaterial-inspired monopole antenna with modified S-shaped resonator," *Progress In Electromagnetics Research Letters*, Vol. 23, 39–48, 2011.
8. Zhao, G., Y. C. Jiao, X. Yang, C. Lin, and Y. Song, "Wideband circularly polarized microstrip antenna using broadband quadrature power splitter based on metamaterial transmission line," *Microw. Opt. Technol. Lett.*, Vol. 51, 1790–1793, 2009.
9. Bernard, L., G. Chertier, and R. Sauleau, "Wideband circularly polarized patch antennas on reactive impedance substrates," *IEEE Antennas Wirel. Propag. Lett.*, Vol. 10, 1015–1018, 2011.

10. Kossiavas, C., A. Zeitler, G. Clementi, C. Migliaccio, R. Staraj, and G. Kossiavas, "X-Band circularly polarized antenna gain enhancement with metamaterials," *Microw. Opt. Technol. Lett.*, Vol. 53, 1911–1915, 2011.
11. Zarifi, D., H. Oraizi, and M. Soleimani, "Improved performance of circularly polarized antenna using semi-planar chiral metamaterial covers," *Progress In Electromagnetics Research*, Vol. 123, 337–354, 2012.
12. Hosseininnejad, S. E., N. Komjani, D. Zarifi, and M. Rajabi, "Directivity enhancement of circularly polarized microstrip antennas by chiral metamaterial covers," *IEICE Electronics Express*, Vol. 9, 117–121, 2012.
13. Zhao, G., Y. C. Jiao, F. Zhang, and X. Yang, "High gain circularly polarized antenna using sub-wavelength resonant cavity," *Journal of Electromagnetic Waves and Applications*, Vol. 24, No. 1, 33–40, 2010.
14. An, J., G. M. Wang, C. X. Zhang, and H. Y. Zeng, "A compact, omni-directional, circularly polarized microstrip antenna," *Microwave Journal*, Vol. 53, 82-+, Jan. 2010.
15. Park, B. C. and J. H. Lee, "Omnidirectional circularly polarized antenna utilizing zeroth-order resonance of epsilon negative transmission line," *IEEE Trans. on Antennas and Propag.*, Vol. 59, 2717–2720, 2011.
16. Park, B. C. and J. H. Lee, "Dual-band omnidirectional circularly polarized antenna using zeroth- and first-order modes," *IEEE Antennas Wirel. Propag. Lett.*, Vol. 11, 407–410, 2012.
17. Herraiz-Martinez, F. J., E. Ugarte-Munoz, V. Gonzalez-Posadas, L. E. Garcia-Munoz, and D. Segovia-Vargas, "Self-diplexed patch antennas based on metamaterials for active RFID systems," *IEEE Trans. on Microw. Theory and Tech.*, Vol. 57, 1330–1340, 2009.
18. Cao, W. Q., B. N. Zhang, T. B. Yu, A. J. Liu, S. J. Zhao, D. S. Guo, and Z. D. Song, "Single-Feed Dual-band dual-mode and dual-polarized microstrip antenna based on metamaterial structure," *Journal of Electromagnetic Waves and Applications*, Vol. 25, No. 13, 1909–1919, 2011.
19. Dong, Y. D., H. Toyao, and T. Itoh, "Compact circularly-polarized patch antenna loaded with metamaterial structures," *IEEE Trans. on Antennas and Propag.*, Vol. 59, 4329–4333, 2011.
20. Jung, Y. K. and B. Lee, "Dual-band circularly polarized microstrip RFID reader antenna using metamaterial branch-line coupler," *IEEE Trans. on Antennas and Propag.*, Vol. 60, 786–791, 2012.

21. Yu, A., F. Yang, and A. Z. Elsherbeni, "A dual band circularly polarized ring antenna based on composite right and left handed metamaterials," *Progress In Electromagnetics Research*, Vol. 78, 73–81, 2008.
22. Zhang, H., Y. Q. Li, X. Chen, Y. Q. Fu, and N. C. Yuan, "Design of circular/dual-frequency linear polarization antennas based on the anisotropic complementary split ring resonator," *IEEE Trans. on Antennas and Propag.*, Vol. 57, 3352–3355, 2009.
23. Dong, Y. D., H. Toyao, and T. Itoh, "Design and characterization of miniaturized patch antennas loaded with complementary split-ring resonators," *IEEE Trans. on Antennas and Propag.*, Vol. 60, 772–785, 2012.
24. Zhou, L., S. Liu, Y. Wei, Y. Chen, and N. Gao, "Dual-band circularly-polarised antenna based on complementary two turns spiral resonator," *Electron. Lett.*, Vol. 46, 970–U26, 2010.
25. Jin, P. and R. W. Ziolkowski, "Multi-frequency, linear and circular polarized, metamaterial-inspired, near-field resonant parasitic antennas," *IEEE Trans. on Antennas and Propag.*, Vol. 59, 1446–1459, 2011.
26. Cao, W. Q., B. N. Zhang, A. J. Liu, T. B. Yu, D. S. Guo, and K. G. Pan, "A reconfigurable microstrip antenna with radiation pattern selectivity and polarization diversity," *IEEE Antennas and Wireless Propagation Letters*, Vol. 11, 453–456, 2012.
27. Herraiz-Martínez, F. J., V. González-Posadas, L. E. Garcia-Munoz, and D. Segovia-Vargas, "Multifrequency and dual-mode patch antennas partially filled with left-handed structures," *IEEE Trans. on Antennas and Propag.*, Vol. 56, No. 8, 2527–2539, Aug. 2008.
28. Wong, K.-L., *Compact and Broadband Microstrip Antennas*, John Wiley & Sons, New York, 2002.
29. Xu, H.-X., G.-M. Wang, and J.-Q. Gong, "Compact Dual-Band Zeroth-Order Resonance Antenna," *Chinese Physics Letters*, Vol. 29, 014101, 2012.